VOLUMEN 48
XXXI Verano De la Ciencia
ISSN 2395-9797
www.jovenesenlaciencia.ugto.mx

Removal of textile dyes from the liquid phase using alternative *Tenebrio molitor* feces–alginate-based biomaterials in fixed-bed columns

Remoción de colorantes textiles en fase líquida sobre biomateriales alternativos a base de heces de *Tenebrio molitor*-alginato mediante columnas de lecho fijo

Ana Pamela Fuerte Aguilar[1], Carlos Esteban Banda Martínez[1], Zahir Muñoz Godoy[1], José Luis Zárate Castrejón[1] , Vicente Peña Caballero[1*]

[1]Universidad de Guanajuato, Campus Celaya-Salvatierra, DCSI, Departamento de Ingeniería Agroindustrial, Sede Mutualismo, Programa Educativo de Licenciatura en Ingeniería en Biotecnología. Sección de Análisis Dinámico de Bioprocesos, Laboratorio de Investigación en Biotecnología. Prolongación Río Lerma s/n, Col. Suiza, C.P. 38060
vicente.caballero@ugto.mx [1*]

Abstract

Packed-bed column adsorption is a continuous process in which mass transfer occurs between the mobile phase containing the adsorbate and the solid phase of the packed bed. This study evaluated the adsorption performance of sodium alginate hydrogel beads encapsulating *Tenebrio molitor* feces for the removal of a commercial dye under continuous-flow conditions. A methodology for the encapsulation of the feces in sodium alginate was developed, and adsorption experiments were conducted at two flow rates and different bed heights. The experimental data were used to estimate the kinetic parameters of Adams-Bohart's model and describe the breakthrough behavior of the system. The encapsulated biomaterial exhibited a moderate increase in the breakthrough service time compared with the control. In addition, the Adams-Bohart's model adequately predicted the breakthrough curves under the evaluated operating conditions, demonstrating its suitability for describing the adsorption performance of the packed-bed system.

Palabras clave: *Tenebrio molitor*, column-adsorption, fixed-bed, dyes.

Introduction

Water pollution has become one of the most critical environmental challenges worldwide, driven by increasing domestic and industrial exploitation, groundwater depletion, and the continuous discharge of untreated wastewater. Among industrial sectors, the textile industry is one of the largest contributors to environmental pollution, accounting for approximately 10% of global greenhouse gas emissions and consuming nearly 215 billion liters of water annually (UNECE, 2026). It is also the primary industrial source of synthetic dyes in wastewater, largely due to the release of unfixed dyes during textile manufacturing (Pérez, 2024). According to the World Bank, textile production is responsible for approximately 20% of global water pollution, with the dyeing process representing the main source of contamination. During this stage, 10–25% of the applied dye fails to bind to textile fibers, resulting in the discharge of approximately 16% of the initial dye load into wastewater streams (Khan, 2022). These findings highlight the urgent need for effective strategies to mitigate dye-contaminated effluents.

Synthetic dyes are highly ecotoxic compounds that are commonly classified according to the chemical structure of their chromophore groups or their application method. Among them, azo and anthraquinone dyes are the most widely used in the textile industry because of their versatility, strong fiber affinity, and compatibility with multiple dyeing processes. Their interactions with textile fibers also determine their environmental fate: reactive dyes form stable covalent bonds that enhance resistance to degradation and generate potentially hazardous by-products, whereas disperse and direct dyes exhibit greater mobility in aqueous effluents. Azo dyes are of particular concern due to their mutagenic and carcinogenic potential, high chemical stability, resistance to biodegradation, and tendency to bioaccumulate and biomagnify within food webs. Their nitrogen-containing chromophores may also contribute to eutrophication by promoting excessive plant growth (Zaruma, 2018). Likewise, acid, direct, and sulfur dyes have been reported to exert toxic effects on aquatic organisms and pose risks to human health, especially through dermal and ocular exposure. Although ecosystems

possess a remarkable capacity to adapt to complex pollutants, their resilience is increasingly threatened by the continuous discharge and variable composition of contaminated effluents (Bundschuh, 2023**).** Accordingly, the development of efficient wastewater treatment technologies remains essential to reduce the release of toxic contaminants into aquatic and terrestrial ecosystems. Various treatment methods, including membrane separation, coagulation–flocculation, adsorption, precipitation, ion exchange, and bioremediation, have been investigated for dye removal from wastewater (Rendón, 2024). Although each technique has limitations related to efficiency, cost, scalability, or operational constraints (Khan, 2022), adsorption has gained particular attention because of its high removal efficiency, simple operation, low cost, and the potential to employ reusable or waste-derived adsorbents, such as valorized agro-industrial residues. Compared with other treatment technologies, fixed-bed column adsorption offers several advantages, including ease of scale-up, continuous operation, and the absence of secondary pollutant generation, making it a sustainable and practical option for industrial applications (Patel, 2019).

Numerous mathematical models have been developed to predict adsorption performance. Among the available approaches, the Thomas, Yoon–Nelson, and Bed Depth Service Time (BDST) models are the most applied to fixed-bed columns. Although these models neglect intraparticle diffusion, they provide reliable predictions by assuming that external film diffusion and surface reaction kinetics control the adsorption process (Patel, 2019). However, experimental validation remains essential for optimizing design and operating conditions, particularly during scale-up. Kinetic analyses provide key parameters, such as breakthrough time, saturation time, adsorption capacity, and rate constants, which are critical for predicting system behavior under dynamic conditions.

Most adsorption studies are traditionally performed in batch systems, in which a fixed quantity of adsorbent is brought into contact with a solution containing a known concentration of contaminant until adsorption equilibrium is attained. In contrast, fixed-bed column adsorption is carried out under continuous-flow conditions, generating a dynamic mass transfer process between the liquid phase (adsorbate) and the solid phase (adsorbent bed). This operating mode more closely represents industrial wastewater treatment systems while allowing continuous evaluation of adsorption behavior throughout the process. As the column operates, the mass transfer zone gradually advances through the adsorbent bed until saturation is reached. At this stage, the contaminant concentration in the effluent begins to increase and eventually approaches the influent concentration. A fundamental parameter in fixed-bed adsorption is the breakthrough time, defined as the moment when the effluent concentration reaches 10% of the influent concentration. The adsorption performance is commonly represented by a breakthrough curve, which relates the normalized concentration ratio (C/C_0) to time. These breakthrough curves are widely used to assess adsorption efficiency and compare system performance under different operating conditions.

With the rise of environmental biotechnology, bioadsorption processes have been widely reported in recent decades for a wide variety of pollutants, as well as using various biological systems and/or their derivatives. Insects, primarily their exoskeletons, have been employed as bioadsorbent materials. Kyzioł-Komosińska et al. (2023) reported the removal of the anionic dyes Reactive Black 5 (RB5) and Reactive Yellow 84 (RY84), as well as the cationic dyes Basic Violet 10 (BV10) and Basic Red 46 (BR46), using chitin extracted from the molts of *Tenebrio molitor* as the adsorbent. Nevertheless, Azzi et al. (2024) produced chitosan through the alkaline deacetylation of chitin extracted from different life stages of *Tenebrio molitor*, demonstrating that this insect represents a promising alternative source of chitin and chitosan. Both chitosan and chitin are biopolymers that have been extensively obtained from organisms such as shrimp, crabs, and squid for the removal of a wide variety of textile dyes, including methylene blue (Vakili et al., 2014) also Congo red, Reactive Black 5 and Reactive Yellow 145 at Crini et al. reported in 2021), among many others.

At present, studies investigating the use of *Tenebrio molitor* feces as a bioadsorbent are scarce; therefore, the present study provides a foundation for future research in this field. However, dried beads and/or sodium alginate hydrogels have been widely reported as polymeric matrices for immobilizing a broad range of biomaterials in adsorption processes. For example, the efficient adsorption of textile dyes such as Congo red has been demonstrated using immobilized *Chlorella* sp. biomass and the fungus *Pleurotus djamor* (Martínez, 2012; Escalante, 2025). Likewise, FD&C Blue No. 1 and FD&C Red No. 40 have been successfully adsorbed using immobilized agro-industrial residues, including fish scales, corn cobs, and corn bracts (Santos, 2022). In addition, methylene blue adsorption has been largely reported using biochar derived from agro-industrial wastes, such as sugarcane bagasse, woody residues, and mushroom substrates, among others.

This study aimed to evaluate the performance of a continuous adsorption system using a fixed-bed column (packed bed) under diverse experimental settings. Specifically, the influence of initial dye concentration, volumetric flow rate, and bed height on removal efficiency was investigated. The target pollutant was a commercial textile dye (PUTNAM®), predominantly composed of Direct Blue 86, and the adsorbent media consisted of sodium alginate-based hydrogel beads. Finally, the experimental results were fitted to a kinetic model to estimate key performance parameters and validate the operational applicability of the column system under the selected conditions.

Materials and methods

Biological material

The feces was isolated from the spent substrate of a Tenebrio molitor culture adapted to laboratory conditions (A). Subsequently, the substrate was sieved, and the fraction retaining the frass (250 µm) was isolated and ground, as it exhibited a uniform size and shape. The ground frass was then sieved to obtain a fraction with a particle size between 38 µm and 50 µm (38 µm < x < 50 µm).

Alginate solution preparation

Sodium alginate solution (3% w/v) was made by incrementally adding sodium salt (Meyer ®) of alginate into beakers containing distilled water. An overhead mechanical stirrer (Cole-Parmer) was placed over the beaker at 200 rpm; gradually all sodium alginate is added. It is imperative to sterilize the solution to achieve complete dissolution (i.e., viscous, clear solution, any bubbles) (Ashvin et al., 2024).

Small sodium alginate hydrogel beads preparation

Alginate reticulation method by calcium ions (Ruiz-Marin et al., 2010; Siripattanakul and Khan, 2010) was used to prepare sodium alginate (SA) hydrogel beads (SAHB) with an average spherical diameter of 0.4–0.5 mm. SAHB were made by dripping the SA (*3% w/v*) into 3% (*w/v*) sterile calcium chloride solution. The Ca^{2+} plays a key role in the cross-linking of the alginate polymer to form a solid bead. After overnight hardening, SAHB were rinsed twice with sterilized and once with distilled water. Figure 1 shows a flowchart of the process from the manufacture of the SAHBs to the assembly of the system.



Figure 1. Experimental overview of Tenebrio molitor's feces encapsulation in small sodium alginate hydrogel beads (SAHB). AI-generated images created with Illustrae.co using our own photo files.

Adsorption Test

The hydrogels were introduced into plastic tubes with a capacity of 90 mL and an internal diameter of ~1.4 cm. The inlet and outlet nozzles were designed using 3D printing to fit the diameter of the columns. The present study employed an experimental design with two factors: bed height and volumetric flow rate, respectively. The columns were filled with hydrogels up to the corresponding bed height, mounted on a universal support, and connected at both ends to a tubing system driven by a peristaltic pump, which simultaneously supplied the flow to all columns.The adsorption experiment was carried out in a four-column fixed bed for each system with SAHB (control and with feces) and at different bed height Z (*see* ***Table*** **1** *and* **2**)as shown in Figure 1 (experimental scheme of column study). In addition, the fixed parameters used were 10 ppm inlet concentration (C0) of blue commercial dye (El Caballito®), the liquid flow Qv (Qv =1.0 and Qv =0.5 L/min) controlled by a peristaltic pump (Masterflex L/S, Model 7523-90 by Col-Parmer) using Cole-Parmer Masterflex Multichannel 4-Ch Peristaltic Pump 7523-80 & two heads 7536-04. The system was run at temperature ≈25ºC and constant pH, evaluating at the same liquid flow, the performance of two heights (Z), each of them had four repeats.

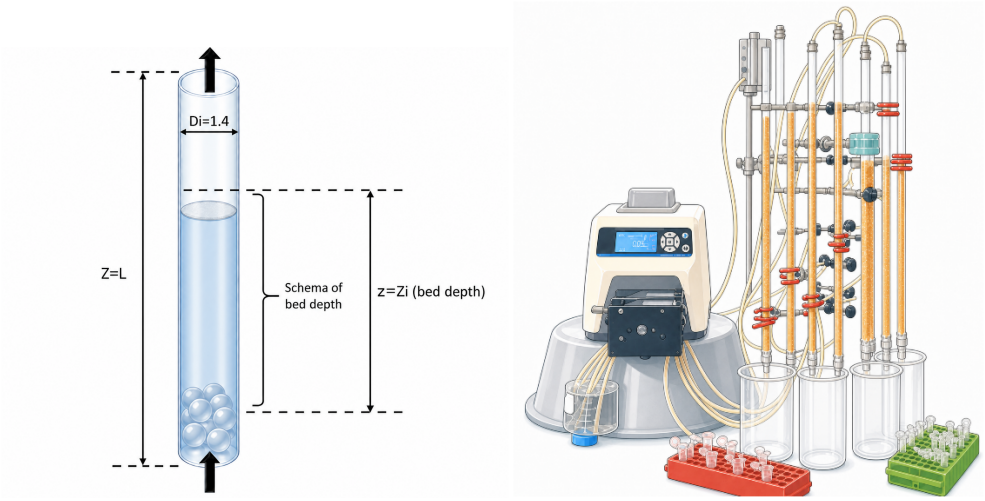

Figure 2. Experimental scheme of column study. AI-generated images created with Illustrae.co using our own photo files.

Adsorption modeling

The adsorption test was analyzed throughout Adams-Bohart's model in 1920. (ecuation 1a), different parameters were derived from model which described the performance of the adsorption column (ecuation 3). The linear and nonlinear adsorption model is described as follows (2 and 1a, respectively).

$$\frac{C_t}{C_0} = \frac{1}{1 + e^{\left(\frac{k_{ads} z N_0}{U} - k_{ads} C_0 t\right)}} \tag{1a}$$

or

$$y = \frac{1}{1 + e^{[k_{ads}(a - bx)]}} \tag{1b}$$

Where $a = \frac{zN_0}{U}$, $b = C_0$, $y = \frac{C_t}{C_0}$, and $x = t$

Now, for simplicity, the linear version of the nonlinear model in equation (2) is as follows:

$$ln\left(\frac{C_0}{C_b} - 1\right) = ln\left(e^{\left(k_{ads} N_0 \left(\frac{z}{U}\right)\right)} - 1\right) - k_{ads} C_0 t_b \tag{2}$$

Where t_b is the service time at breakthrough point (min), $N_0$the dynamic bed capacity (mg L-1), z the packed-bed column depth (m), U: the linear flow rate (m min-1) defined as the ratio of the volumetric flow rate Q_v (m3 min-1), to the cross-sectional area of the bed S_c (m2), C_0 and $C_b$are, respectively, the inlet and the breakthrough colorant ions concentration (mg L-1) and k_{ads} the adsorption rate constant (L-1mg-1 min). Equation (2) known under the name of bed depth service time (BDST) can be determined for a given adsorbent depth and is a straight line (Hutchins, 1973):

$$\overbrace{\underbrace{t_{b_i} = \left[\frac{N_0}{C_0 U}\right] z_i - \left[\frac{1}{k_{ads} C_0}\right] ln\left(\frac{C_0}{C_b} - 1\right)}_{\text{relación lineal entre la profundidad del lecho de la columna } (z) \text{ y tiempo de servicio } (t_b)} \rightarrow}^{\text{Bed depth service time (BDST)}} \quad \underbrace{y_i = \beta_0 + \beta_1 x_i; i = 1, 2, \ldots, n}_{\text{Bed height versus time}}: \tag{3}$$

$$\Rightarrow \begin{cases} y_i = t_{b_i} \\ \beta_0 = \left[\frac{1}{k_{ads} C_0}\right] ln\left(\frac{C_0}{C_b} - 1\right) \\ \beta_1 = \left[\frac{N_0}{C_0 U}\right] \\ x_i = z_i \end{cases}$$

Equation (3) is satisfied if it is verified in equation (2) that: $e^{\left(k_{ads} N_0 \left(\frac{z}{U}\right)\right)} \gg 1$ thus $ln\left(e^{\left(k_{ads} N_0 \left(\frac{z}{U}\right)\right)} - 1\right) \cong k_{ads} N_0 \left(\frac{z}{U}\right)$. Then, from equations (3), $\beta_0 (min)$ and $\beta_1 (min\, m^{-1})$, respectively, is the slope of the BDST line and represents the time required for the adsorption zone to travel a unit length through the adsorbent and is the abscissa intercept in the BDST plot and the dynamic bed capacity (N_0) and the adsorption rate constant (k_{ads}) can be evaluated from the slope and intercept of the plot of t_{b_i} versus z_i: $N_0 = \beta_1 C_0 U$ and $k_{ads} = \left[\frac{1}{\beta_0 C_0}\right] ln\left(\frac{C_0}{C_b} - 1\right)$ (see appendix A: a fast algorithm to solve systems of linear equations, e.i., equation (2)).

Remark ($z_{i=0} = z_0$). The bed depth (z_0), which represents the theoretical depth of SSAHB able to prevent the adsorbent concentration from exceeding C_b , is obtained when $t_b = 0$ (see equation (3)), according to the following equation:

$$0 = \left[\frac{N_0}{C_0 U}\right] z_0 - \left[\frac{1}{k_{ads} C_0}\right] ln\left(\frac{C_0}{C_b} - 1\right) \rightarrow z_0 = \left[\frac{U}{N_0 k_{ads}}\right] ln\left(\frac{C_0}{C_b} - 1\right) \quad (3) \tag{4}$$

The reader is referred to Patel, et al. (2019) for further details of models available in the literature for linear modeling of packed bed columns or design of the adsorption column based on bed depth service time.

Results and Discussion

Bioadsorbents: Immobilization of *T. molitor* Feces in Sodium Alginate Hydrogels

The results of the immobilization of *T. molitor* feces in hydrogels are presented in Figure 2 to compare the different approaches and identify the appropriate method for preparing the sodium alginate solution containing the feces. Sterilization of the feces is essential to reduce the environmental microbial load as well as that originating from the insect gut microbiome. Otherwise, there is a risk of contamination of both the hydrogels and the 6% $CaCl_2$ solutions due to the organic matter present in the feces and the aqueous environment in which they are prepared. To prevent contamination, each $CaCl_2$ solution undergoes a sterilization process and contains the antibiotic chloramphenicol.Sterilization of the feces dispersed in the sodium alginate solution (A) was evaluated in comparison with the method employed in the present study (B), in which the 3% sodium alginate solution and the feces were sterilized separately and subsequently mixed under a laminar flow hood. The morphology (size, surface roughness, and shape) of the hydrogels obtained using method **A** changed considerably due to alterations in the physical (viscosity and precipitate formation) and chemical properties of sodium alginate, likely resulting from Maillard reactions between carbohydrates and proteins present in the feces under the high-temperature and high-pressure conditions of the sterilization process. In contrast, when the biomaterials were sterilized separately using method **B**, spherical and uniform hydrogels were obtained. In addition, the feces remained homogeneously dispersed and suspended in the solution without requiring agitation because of the viscosity of the sodium alginate. In Figure 2, uppercase letters represent the macroscopic appearance, whereas lowercase letters correspond to three-dimensional stereomicroscope images showing the roughness of beads' surface.

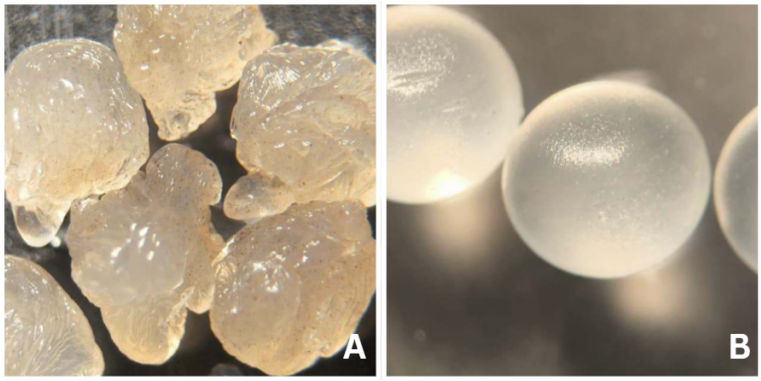

Figure 3. Macroscopic and microscopic views of feces immobilized in sodium alginate hydrogels.

Calibration curve

Linear regression analysis of the calibration curve data yielded the following equation: $y = 840.8x - 0.01981$, as shown in Figure 4. The calibration curve exhibited a high coefficient of determination ($R^2 = 0.9935$), indicating a strong linear relationship between absorbance and dye concentration. Consequently, the calibration curve serves as a reliable reference for validating the dynamic changes in dye concentration within the samples.

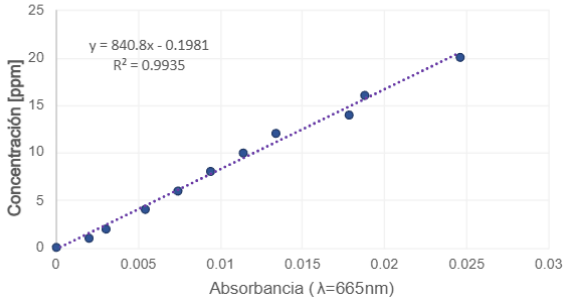

Figure. 4. Calibration curve for the commercial dye PUTNAM®

Adsorption Test

Effect of bed depth and inlet concentration

In the design of fixed-bed column systems, the geometric dimensions of the system establish the basis for scale-up. Tables 1 and 2 present the main parameters related to bed height (Z), the relatively uniform internal diameter among the columns (Di), and the cross-sectional area through which the fluid flows across the system. Likewise, the tables include the maximum allowable concentration established by regulatory standards. (C_b) and the concentration of nutrients in each column (C_0).

Table 1 Geometric dimensions for flow (mL/min) and bed depth (m) at four-column fixed bed system with SAHB (Negative Control).

				Flow $[mL\ min^{-1}]$			
				0.5		1	
Z $[m]$		D_i $[m]$	S_c $[m^2]$	C_0 $[mg\ L^{-1}]$	C_b $[mg\ L^{-1}]$	C_0 $[mg\ L^{-1}]$	C_b $[mg\ L^{-1}]$
$^1/_4$	0.1135	0.0143	0.000161	10.7323	0.9230	10.1718	0.9230
$^1/_2$	0.1980	0.0141	0.000156	10.1718	1.7638	10.1718	1.2032
$^3/_4$	0.3248	0.0145	0.000165	10.1718	0.9230	9.6112	1.7638

4/4	0.3975	0.0143	0.000161	10.2839	1.5956	10.2839	1.0351

Note: Z: Column's height; D_i :Inner diameter; S_c: cross-sectional area of the bed;C_0 and $C_b$are, respectively, the inlet and the breakthrough colorant concentration $[mg\ L^{-1}]$.

Table 2. Geometric dimensions for flow (mL/min) and bed depth (m) at four-column fixed bed system with SAHB + *Tenebrio molitor* feces.

				Flow $[mL\ min^{-1}]$			
				0.5		1	
Z $[m]$		D_i $[m]$	S_c $[m^2]$	C_0 $[mg\ L^{-1}]$	C_b $[mg\ L^{-1}]$	C_0 $[mg\ L^{-1}]$	C_b $[mg\ L^{-1}]$
1/4	0.1113	0.0143	0.000161	10.1718	0.9230	9.8915	1.7638
1/2	0.1974	0.0141	0.000156	10.4520	1.2032	10.1718	0.9230
3/4	0.3225	0.0145	0.000165	10.1718	1.4835	10.4520	1.2032
4/4	0.3990	0.0143	0.000161	10.1718	1.2032	10.4520	0.9230

Note: Z: Column's height; D_i :Inner diameter; S_c: cross-sectional area of the bed;C_0 and $C_b$are, respectively, the inlet and the breakthrough colorant concentration $[mg\ L^{-1}]$.

Gráfica t_{bi} vs Z_i

The breakthrough curves obtained for blue dye adsorption are demonstrated in *Figure 5* for different bed depth of SAHB (control) at a constant flow rate of: A) 0.5 and B) 1 mL/min.

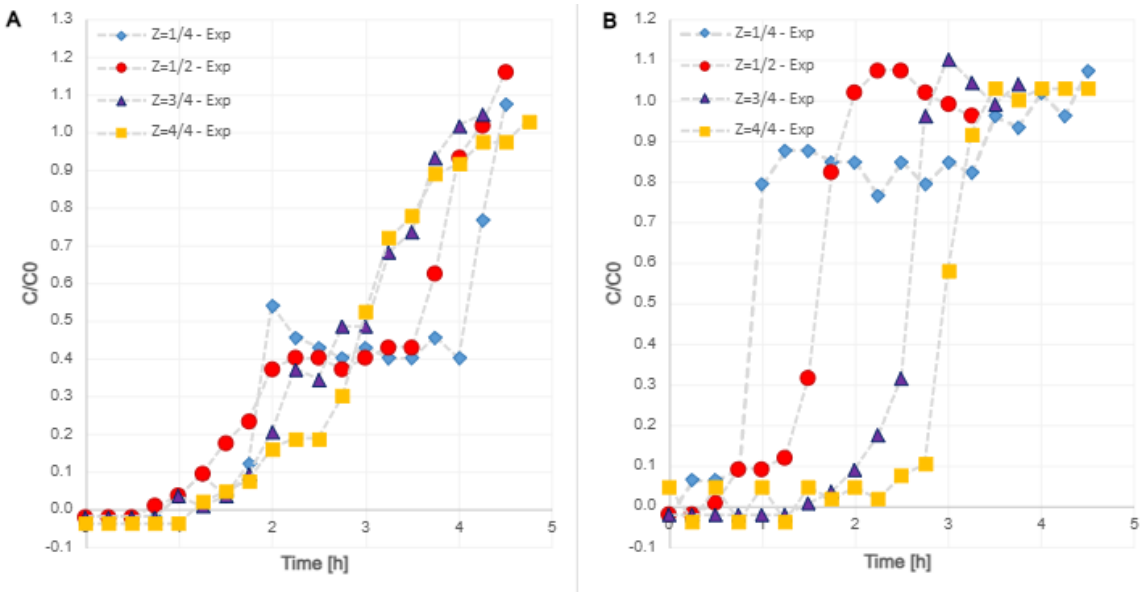

Figure 5. Adsorption test of four-columns fixed bed system with SAHB (control)

Note: Break point curves of PUTNAM® dye at two flow rates (A: 0.5 mL/min; B: 1 mL/min) and bed depth (Z_1, Z_2 , Z_3 and Z_4).

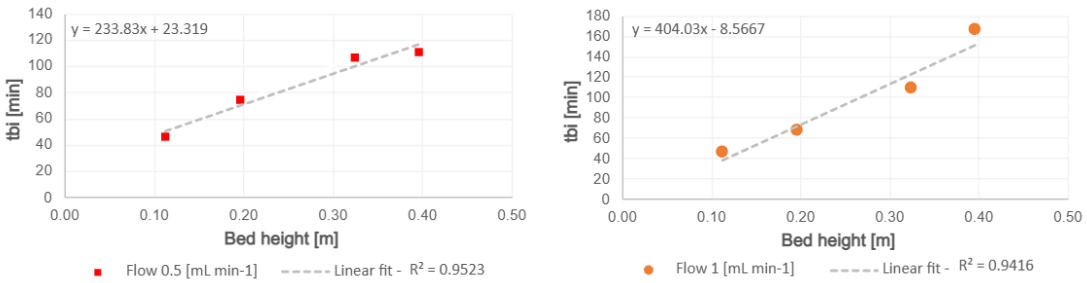

Figure 6. Linear regression of depth's service time at breakthrough points of SAHB (control).

Note: Red and orange marks represent respectively the flows 0.5 and 1 mL/min, in gray is showed the Linear fitting for each one.

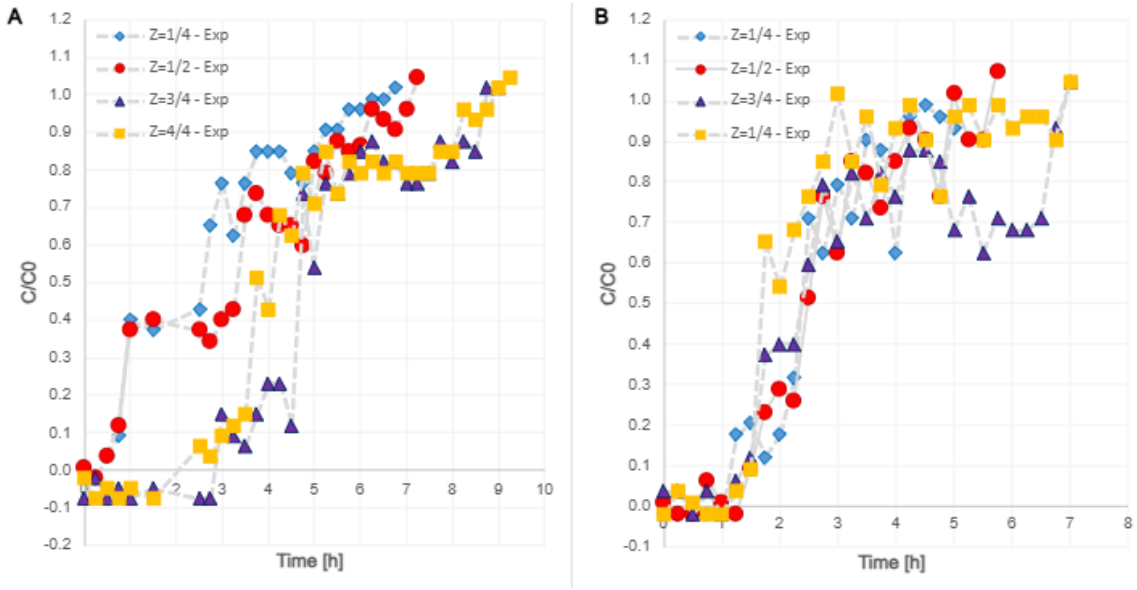

Figure 7. Adsorption test of four-columns fixed bed system with SAHB + Tenebrio molitor feces.
Note: Break point curves of PUTNAM® dye at two flow rates (A: 0.5 mL/min; B: 1 mL/min) and bed depth (Z_1, Z_2 , Z_3 and Z_4).

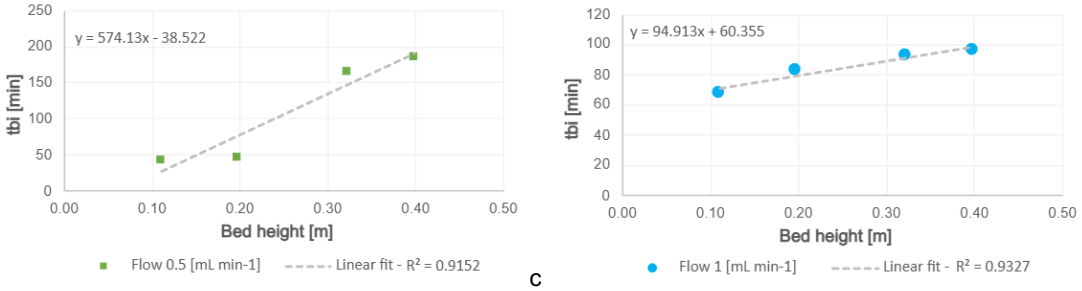

C

Figure 8. Linear regression of depth's service time at breakthrough points of SAHB + Tenebrio molitor feces.

The breakthrough curves show that the time required to reach the breakthrough point depends on the bed height, as shorter beds reach the influent concentration more rapidly. The saturation times were relatively similar because the differences in bed heights were not substantial. Nevertheless, the experiments clearly demonstrated that taller beds required longer times to reach the breakthrough point.

Adsorption modeling

From the experimental adsorption data $\left({}^{C}/_{C_0}\right)$, the service time at the breakthrough point (t_{bi}), was determined, corresponding to the time at which the effluent reaches 10% of the influent concentration (i.e., if $(if\ C_0 \approx 10\ ppm,\ then\ C_b \cong 1ppm)$.. In the design of fixed-bed columns (t_{bi}), represents the operating time during which the column can function before the biomaterials become saturated. Beyond this point, the effluent concentration exceeds the regulatory limit (~1 ppm) and gradually approaches the influent concentration $C_0 \approx 10\ ppm$). Since the service time is directly proportional to the bed height, the saturation time increases as the bed height increases. Linear regression of the t_{bi} values yielded the slope (m) and intercept (b), which were subsequently fitted to the linearized Adams-Bohart's model to determine the kinetic parameters required for scaling up the system. The following tables present the results obtained from the determination of these

parameters based on the adsorption behavior of the control system and the treatment system (SAHB + *Tenebrio molitor* feces).

Table 4. Model parameters calculated for flow and bed depth at four-column fixed bed system with SAHB (Negative Control).

Flow $[mL\ min^{-1}]$	0.5		1	
Z $[m]$	N_0 $[mg\ L^{-1}]$	k_{ads} $[min\ [mgL]^{-1}]$	N_0 $[mg\ L^{-1}]$	k_{ads} $[min[mgL]^{-1}]$
0.1135	7.8127	-0.0094	25.5887	0.0264
0.1980	7.6162	-0.0066	26.3198	0.0231
0.3248	7.2018	-0.0097	23.5162	0.0181
0.3975	7.4863	-0.0071	25.8708	0.0249

Note: Parameters obtained from the regression using the Bohart-Adams model' linearized. Fluxes were used as $[m^3\ min^{-1}]$ instead of $[mL\ min^{-1}]$ to dimensional accordance.

Table 5. Model parameters calculated for flow and bed depth at four-column fixed bed system with SAHB + *Tenebrio molitor* feces.

Flow $[mL\ min^{-1}]$	0.5		1	
Z $[m]$	N_0 $[mg\ L^{-1}]$	k_{ads} $[min\ [mgL]^{-1}]$	N_0 $[mg\ L^{-1}]$	k_{ads} $[min[mgL]^{-1}]$
0.1113	18.1810	0.0059	5.8455	-0.0026
0.1974	19.2157	0.0051	6.1829	-0.0038
0.3225	17.6829	0.0045	6.0076	-0.0032
0.3990	18.1810	0.0051	6.1768	-0.0037

Note: All parameters were calculated using the Bohart-Adams model' linearized. Fluxes were used as $[m^3\ min^{-1}]$ instead of $[mL\ min^{-1}]$ to dimensional accordance.

Table 6. Parameters calculated for flow and column fixed bed system with SAHB (Negative Control).

Flow $[mL\ min^{-1}]$	0.5		1	
Z $[m]$	U $[mg\ min^{-1}]$	a $[mg\ min[\ L]^{-1}]$	U $[mg\ min^{-1}]$	a $[mg\ min[\ L]^{-1}]$
0.1135	0.0031	284.8326	0.0062	466.4517
0.1980	0.0032	470.8178	0.0064	813.5164
0.3248	0.0030	772.5860	0.0061	1261.3714
0.3975	0.0031	955.8011	0.0062	1651.5090

Note: Parameters obtained from the regression using the Bohart-Adams model' linearized. Fluxes were used as $[m^3\ min^{-1}]$ instead of $[mL\ min^{-1}]$ to dimensional accordance.

Table 7. Parameters calculated for flow and column fixed bed system with SAHB + *Tenebrio molitor* feces.

Flow $[mL\ min^{-1}]$	0.5		1	
Z $[m]$	U $[mg\ min^{-1}]$	a $[mg\ min[\ L]^{-1}]$	U $[mg\ min^{-1}]$	a $[mg\ min[\ L]^{-1}]$
0.1113	0.0031	649.9873	0.0062	104.4915
0.1974	0.0032	1184.7214	0.0064	190.5996
0.3225	0.0030	1883.5323	0.0061	319.9541
0.3990	0.0031	2329.9971	0.0062	395.7947

Note: All parameters were calculated using the Bohart-Adams model' linearized. Fluxes were used as $[m^3\ min^{-1}]$ instead of $[mL\ min^{-1}]$ to dimensional accordance.

These parameters are essential for evaluating the efficiency of the system and comparing its performance under different operating conditions.

Conclusion

It is recommended to standardize commercial dyes through a pretreatment process to reduce analytical interferences. The use of commercial textile dyes provides the opportunity to evaluate a representative contaminant commonly found in domestic wastewater. However, it also presents experimental challenges due to their undisclosed composition, as manufacturers protect their production processes and/or formulations. In a preliminary study published in 2025 (Fuerte et. al., 2025), the use of dyes without incorporated fixatives was recommended because of the difficulty in separating the pigment from the mordant. Nevertheless, regardless of whether fixatives are included, commercial pigments are formulated with undeclared ingredients or contain impurities resulting from insufficient purification processes. Furthermore, the dye solution prepared with distilled water and stored in an amber container remains stable for approximately 4–5 days. Thereafter, pigment aggregates begin to form and precipitate, thereby altering the actual concentration of the stock solution used for subsequent dilutions.

This study developed a system to produce sodium alginate hydrogels with diameters smaller than 4 mm. The intellectual property protection and advanced characterization of the hydrogels are currently in progress and are reserved for a second phase of the study. The SAHs could represent a promising adsorbent for the tertiary treatment of industrial effluents contaminated with dyes.

References

Ashvin Iresh Fernando, P. U., Kennedy, A. J., Pokrzywinski, K., Jernberg, J., Thornell, T., George, G., Kosgei, G. K., Wang, Y., & Coyne, K. J. (2024). Development of alginate beads for precise environmental release applications: A design of experiment based approach and analysis. *Journal of Environmental Management, 351*, 119872. https://doi.org/10.1016/j.jenvman.2023.119872

Azzi, M., Elkadaoui, S., Zim, J., Desbrieres, J., El Hachimi, Y., & Tolaimate, A. (2024). *Tenebrio molitor* breeding rejects as a high source of pure chitin and chitosan: Role of the processes, influence of the life cycle stages and comparison with *Hermetia illucens*. *International Journal of Biological Macromolecules, 277*, 134475. https://doi.org/10.1016/j.ijbiomac.2024.134475

Bohart, G. S., & Adams, E. Q. (1920). Adsorption in columns. *Journal of the American Chemical Society, 42*(3), 523–544.

Bundschuh, M., Mesquita-Joanes, F., Rico, A., & Camacho, A. (2023). Understanding ecological complexity in a chemical stress context: A reflection on recolonization, recovery, and adaptation of aquatic populations and communities. *Environmental Toxicology and Chemistry*, **42**(9), 1857–1866.

Crini, G., et al. (2021). Applications of chitin and chitosan based biomaterials for the adsorptive removal of textile dyes from water—A comprehensive review. *Carbohydrate Polymers, 273*, 118604. https://doi.org/10.1016/j.carbpol.2021.118604

Escalante-García, M. et. al (2015) Uso de hongos inmovilizados en materiales carbonosos para la remoción de colorantes en aguas residuales. *JÓVENES EN LA CIENCIA*, *37*, 1-14. https://doi.org/10.15174/jc.2025.4902

Fuerte Aguilar, A. P, Cerrito Florencio, C. B, Zárate Castrejón, J. L. & Peña Caballero, V. (2025) Preliminary Study of Blue Dye Removal on Small Sodium Alginate Hydrogel Beads in Fixed-Bed Glass Columns: A Basic Experimental and Mathematical Approach. *JÓVENES EN LA CIENCIA*, *37*,, ISSN 2395-9797 www.jovenesenlaciencia.ugto.mx

Hutchins, R. A. (1973). New method simplifies design of activated carbon systems. *American Institute of Chemical Engineers Journal, 80*(4), 133–138.

Khan, A. A., Gul, J., Naqvi, S. R., Ali, I., Farooq, W., Liaqat, R., AlMohamadi, H., Štěpanec, L., & Juchelková, D. (2022). Recent progress in microalgae-derived biochar for the treatment of textile industry wastewater. *Chemosphere, 306*, 135565. https://doi.org/10.1016/j.chemosphere.2022.135565

Kyzioł-Komosińska, J., et al. (2023). The use of chitin from the molts of mealworm (*Tenebrio molitor*) for the removal of anionic and cationic dyes from aqueous solutions. *Molecules, 28*.

Martínez Tristán, A. (2012). BIOSORCIÓN DEL COLORANTE ROJO CONGO EN SISTEMAS EN LOTE UTILIZANDO BIOMASA DE Chlorella sp. UNIVERSIDAD AUTÓNOMA DE NUEVO LEÓN.

Patel, H. (2019). Fixed-bed column adsorption study: A comprehensive review. *Applied Water Science, 9*(45). https://doi.org/10.1007/s13201-019-0927-7

Rendón Castrillón, L., Ramírez Carmona, M., Ocampo López, C., González-López, F., Cuartas Uribe, B., & Mendoza Roca, J. A. (2024). Efficient bioremediation of indigo-dye contaminated textile wastewater using native microorganisms and combined bioaugmentation-biostimulation techniques. *Chemosphere, 353*, 141538. https://doi.org/10.1016/j.chemosphere.2024.141538

Ruiz-Marin, A., Mendoza-Espinosa, L. G., & Stephenson, T. (2010). Growth and nutrient removal in free and immobilized green algae in batch and semi-continuous cultures treating real wastewater. *Bioresource Technology, 101*, 58–64.

Santos, R. (2022). Análisis de la capacidad adsorbente de residuos agroindustriales en la remoción de colorantes. Universidad Dr. José Matías Delgado. URI: http://hdl.handle.net/10972/4417

Siripattanakul, S., & Khan, E. (2010). Fundamentals and applications of entrapped cell bioaugmentation for contaminant removal. In *Emerging Environmental Technologies* (pp. 147–169).

United Nations Economic Commission for Europe (2026). Rethinking materials and systems: UN highlights pathways to more sustainable fashion. https://unece.org/climate-change/press/rethinking-materials-and-systems-un-highlights-pathways-more-sustainable

Vakili, M., Rafatullah, M., Salamatinia, B., Abdullah, A. Z., Ibrahim, M. H., Tan, K. B., Gholami, Z., & Amouzgar, P. (2014). Application of chitosan and its derivatives as adsorbents for dye removal from water and wastewater: A review. *Carbohydrate Polymers, 113*, 115–130. https://doi.org/10.1016/j.carbpol.2014.07.007

Zaruma, P., Proal, J., Hernández, I. C., & Salas, H. I. (2018). Los colorantes textiles industriales y tratamientos óptimos de sus efluentes de agua residual: una breve revisión. *Revista de la Facultad de Ciencias Químicas, 19*, 38–47.

Appendix

List of symbols

t_b	*Service time at breakthrough point (min)*	Q_v	*Volumetric flow rate* ($m^3\ min^{-1}$)
N_0	*The dynamic bed capacity* ($mg\ L^{-1}$)	S_c	*The cross-sectional area of the bed* (m^2),
z	*The packed-bed column depth* (m)	C_0	*The inlet dye concentration* ($mg\ L^{-1}$)
U	*The linear flow rate* ($m\ min^{-1}$), *defined as the ratio of the volumetric flow rate to the cross-sectional area of the bed*	C_t	*The concentration of effluent at time* ($mg\ L^{-1}$)
k_{ads}	*Adsorption rate constant* ($L^{-1}mg^{-1}\ min$).	C_b	*The breakthrough metal ions concentration* ($mg\ L^{-1}$)